

Stable Metal Anode enabled by Porous Lithium Foam with Superior Ion Accessibility

Ahmed M. Hafez, Yucong Jiao, Jianjian Shi, Yi Ma, Daxian Cao, Yuanyue Liu, and Hongli Zhu*

Lithium (Li) metal anodes have attracted much interest recently for high-energy battery applications. However, low coulombic efficiency, infinite volume change, and severe dendrite formation limit their reliable implementation over a wide range. Here, an outstanding stability for a Li metal anode is revealed by designing a highly porous and hollow Li foam. This unique structure is capable of tackling many Li metal problems simultaneously: first, it assures uniform electrolyte distribution over the inner and outer electrode's surface; second, it reduces the local current density by providing a larger electroactive surface area; third, it can accommodate volume expansion and dissipate heat efficiently. Moreover, the structure shows superior stability compared to fully Li covered foam with low porosity, and bulky Li foil electrode counterparts. This Li foam exhibits small overpotential (≈ 25 mV at 4 mA cm^{-2}) and high cycling stability for 160 cycles at 4 mA cm^{-2} . Furthermore, when assembled, the porous Li metal as the anode with LiFePO_4 as the cathode for a full cell, the battery has a high-rate performance of 138 mAh g^{-1} at 0.2 C. The beneficial structure of the Li hollow foam is further studied through density functional theory simulations, which confirms that the porous structure has better charge mobility and more uniform Li deposition.

Li metal stays the most promising electrode, due to its light weight (0.53 g cm^{-3}), low electrochemical potential (-3.04 V vs standard hydrogen electrode), and high specific capacity (3860 mAh g^{-1}).^[1–4] However, Li has some challenges that limit its commercialization as efficient electrode material, which can be attributed to: i) infinite volume change during charging/discharging processes and ii) uncontrollable reaction between Li metal and electrolyte that leads to the formation of nonuniform solid electrolyte interface (SEI) layer with different thickness and morphology.^[5–8]


A lot of effort has been exerted to solve the aforementioned problems for Li metal electrode, including forming a robust, stable SEI layer between the electrode and electrolyte that can reduce the dendrite formation^[9–15]; stabilizing the SEI layer by adding additives to the electrolyte^[16,17]; designing artificial layer at the electrode/electrolyte interface for dendrite inhibition^[4,18]; and increasing salt concentration in the electrolytes.^[19–21]

High energy density is strongly demanded nowadays for batteries in broad applications, such as electric vehicles, portable electronics, aerospace devices, and other electrical equipment. Although lithium-ion batteries (LIBs) are the most widely used batteries in such applications, their energy density is still quite limited. For this reason, numerous efforts have been focused in finding new anode materials as a suitable replacement for the commonly used graphite electrodes in LIBs, including silicon (Si), tin (Sn), lithium (Li) metal, etc. Among these materials,

Although these methods can control the dendrite formation to a certain extent, they are still not able to control the large volume change of Li during charging/discharging process. Another promising approach is to host Li in a confined scaffold so that it can not only reduce the volume change for the electrode but also provide more stable SEI layer during cycling.^[22–29] To achieve this approach, previous studies have shown that thermal infusion of molten Li is the most efficient way for prestoring Li inside hosts, which provides both uniform distribution and low Li nucleation barrier during battery cycling. For instance, Liang et al. introduced a facile method to melt Li inside porous scaffold.^[30] Their structure afforded remarkable battery performance with low interfacial impedance, long cycle stability, high conductive surface area, and stable SEI interface, compared with hostless Li metal electrode counterpart. Also, Lin et al.^[31] reported the synthesis of layered Li-rGO electrode via molten Li infusion, the rGO layer provided electrochemical and mechanical stability for the SEI, and the structure also offered stable scaffold against volume change through continuous Li stripping/plating. Recently, Chi et al.^[32] demonstrated that Li–Ni composite anode could be fabricated by infusing Li with Ni foam host, the structure

A. M. Hafez, Dr. Y. Jiao, Y. Ma, D. Cao, Prof. H. Zhu
Department of Mechanical and Industrial Engineering
Northeastern University
Boston, MA 02115, USA
E-mail: h.zhu@neu.edu

J. Shi, Prof. Y. Liu
Texas Materials Institute and Department of Mechanical Engineering
University of Texas Austin
Austin, TX 78712-159, USA

 The ORCID identification number(s) for the author(s) of this article can be found under <https://doi.org/10.1002/adma.201802156>.

DOI: 10.1002/adma.201802156

showed improved electrochemical performance and better stability. Very recently, Yu et al.^[33] reported that 3D Ni substrate could effectively stabilize Li metal anode, which is achieved by its ability to suppress the formation of “dead” Li and to generate a dense surface passivation layer. These aforementioned studies proved that Li infusion inside host or scaffold provides better electrochemical performance with higher stability. These structures afforded good battery performance with lower interfacial impedance, smaller Li nucleation overpotential, longer cycle stability, and higher coulombic efficiency compared with the hostless bulky Li metal electrode counterpart. However, in these studies, the Li metal fills the host completely, which decreases the overall contact area between the Li and the electrolyte and enhances the possibility of dendrite formation after long cycling. Moreover, the optimum amount of Li infused through these structures has not been thoroughly investigated, which has a critical effect on the performance and stability of the electrode. For instance, in a previous study, it was mentioned that mossy dendrite still exists on the surface of a highly Li-covered 3D scaffold.^[30] This could be attributed to the close similarity between the fully covered Li hosts and their hostless Li electrodes counterparts. In this case to some extent, Li plating/stripping will still show volume change, dendrite formation, and nonuniform distribution for the electrolyte through the scaffold pores, which in this case is totally blocked by the high Li coverage.

Therefore, attention should be taken into account during Li infusion, by evaluating the optimum coverage for Li inside different hosts. Herein, we controlled the Li amount infused into hollow graphene foam while keeping the well-defined 3D host structure intact. Then we studied the effect of porosity on battery performance. Compared with the full coverage, the hierarchical porous structure with the hollow tubular shape is beneficial as it: i) provides internal ion transfer path inside the hollow foam, by which the charging/discharging process takes place not only on the outer surface of the foam but also on the inner surface, simultaneously; ii) enhances ion diffusion throughout the Li foam electrode, which is crucial for better ionic mobility and lower charge carrier impedance; iii) reduces the local current density by providing 3D Li metal structure with large electroactive surface area; iv) uniformly distributes the electrolyte during lithium metal plating/stripping; and v) confines Li in a well-defined structure, which limits the high volume change during cycling. This morphology showed a large impact on the battery performance, as well as its potential to suppress Li dendrites. Attributed to that, the porous Li foam maintained long cycling stability even after more than 160 cycles under the high current density of 4 mA cm⁻² with 1 mAh cm⁻² charge. In addition, when assembled as a negative electrode in a full cell with LiFePO₄ as positive electrode, the porous Li electrode presented five times higher discharge capacity than the Li foil counterpart at 10 C. The experimental and theoretical results in this study revealed the preference of porous Li metal electrode, not only compared with hostless Li electrodes but also compared with fully Li-covered structure. These findings assert that Li infusion should be carefully controlled and adjusted into hosts and 3D scaffolds in order to optimize the performance, and further reveal the capability of using Li metal foam as a highly stable anode for rechargeable batteries.

As mentioned above, previous reports have shown that graphene is a promising choice as host for Li infusion. However, Li infusion inside graphene is challenging due to its high lithiophobicity (Video S1, Supporting Information). Different reports in the literature describe various methods to infuse Li inside lithiophobic materials through surface modifications in order to enhance its wetting properties.^[30,34,35] Based on these studies, we first modified the graphene foam surface using ZnO, which is found to increase the lithiophilicity of graphene (detailed procedure can be found in the Experimental Section). The advantage of this modification is that it allows homogeneous distribution of Li, which has great impact on its performance as electrode, and further gives control on the amount of Li infused into the host. **Figure 1a,c** represent the schematic of fabrication procedure for the Li foam structure. **Figure 1a** shows the graphene structure deposited on Ni foam as a scaffold. However, **Figure 1b** reveals the etching of Ni foam, by which graphene hollow structure is obtained. The final Li foam structure is shown in **Figure 1c**, which is obtained by Li infusion with graphene foam as template.

To reveal the effect of Li coverage on the electrochemical performance and how it affects the stability of the electrode, we used two different morphologies for Li foam in this study. The first structure is Li foam under low coverage, and the other structure is Li foam under high coverage. For low Li foam coverage, the graphene 3D scaffold was placed carefully in contact with freshly molten Li, by which Li gradually intake throughout the structure in about 2 min (Video S2, Supporting Information). For high Li coverage, the graphene foam was placed directly on the top of molten Li, where Li totally covered the whole structure within 30 s, filling all the pores inside the foam. The areal loading for the low coverage was 8 mg cm⁻², with graphene to Li mass ratio of 1:21, on average. While for the high coverage, the areal loading was 35 mg cm⁻², with graphene to Li mass ratio of 1:95, on average. This indicates that Li loading for the low coverage samples is approximately four times less than its highly covered counterparts. The low-covered samples optimize the amount of Li infused through the structure and further reduce the dendrite formation by excluding redundant Li from the electrode. Even though the mass loading in porous foam is smaller, it has high areal energy density due to the higher contact area between Li and electrolyte in unit area.

Figure 1d–f show three different structure morphologies for Li metal electrodes that are thoroughly investigated in this study. Bare Li foil is represented in **Figure 1d**, where limited electrode/electrolyte contact area and nonhomogeneous Li⁺ distribution at the electrode/electrolyte interface are expected, which enhances the dendrite formation, as illustrated in the schematic diagram. The porous structure under high Li coverage is shown in **Figure 1e**. It is obvious that the high coverage of Li inside the structure approximately blocks the pores, which decreases the amount of diffused electrolyte into the structure, and reduces the overall contact area between Li metal surface and electrolyte. **Figure 1f** illustrates the hollow Li foam under low Li coverage. The low-covered foam has significant porosity, which facilitates better electrolyte diffusion inside the structure, and enhances the contact area between Li metal and electrolyte, which increases the charge carrier and

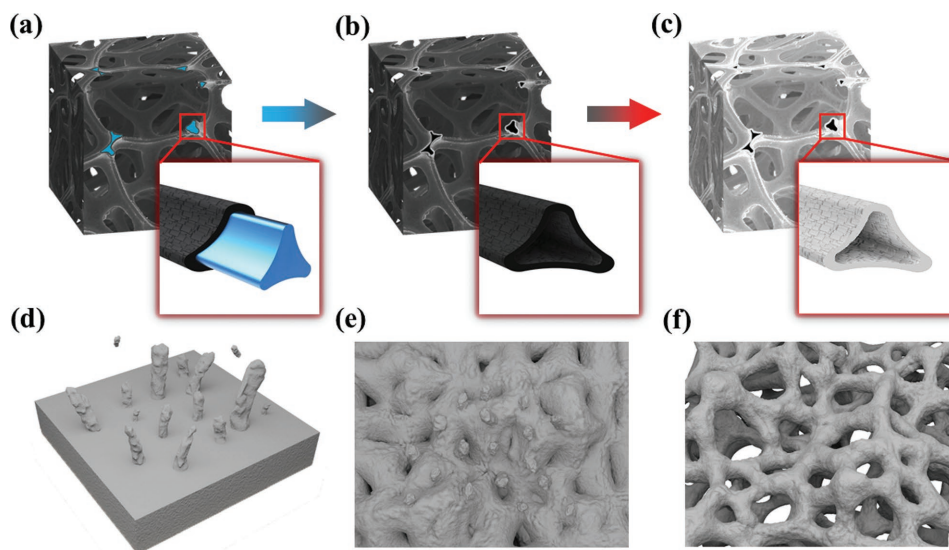


Figure 1. Schematic diagram of the fabrication procedure of Li foam. a) Graphene deposition on Ni foam, b) etching the graphene/Ni foam to obtain hollow graphene foam structure, and c) Li infusion to cover the graphene foam wall boundaries, by which hollow Li foam structure is obtained. Different structure morphologies for Li metal electrodes: d) bare Li foil, e) Li foam under high coverage, and f) Li hollow foam under low coverage.

ionic mobility. Moreover, the unique hollow structure provides smooth and uniform Li coverage, which has a great effect on suppressing dendrite formation by assuring uniform current density distribution and even Li deposition during charging/discharging.

A snapshot for graphene foam used as template for Li infusion is shown in **Figure 2a**. From the scanning electron microscopy (SEM) images for graphene foam before melting Li under low magnification (**Figure 2b**), it can be seen that after etching Ni, the foam still keeps its foamy structure, which is more clear under high magnification (**Figure 2c**), where completely hollow tubular-like structure can be observed. On the other hand, **Figure 2d** shows a snapshot for the free-standing Li metal foam under low coverage after melting Li into the

graphene foam, which is used as a Li metal anode electrode in our study. **Figure 2e** represents SEM image for the Li foam under low magnification, clearly, the foam still holding its structure after Li infusion, which constitutes highly porous hollow free-standing Li foam. It should be mentioned that after Li infusion, the foam shows much higher mechanical stability to be handled for battery cell assembly. Under high magnification (**Figure 2f**), it is obvious that the tubular-like structure is still thoroughly maintained, with wall boundaries totally covered by lithium on both the inner and outer surfaces. The thickness of the Li wall is 5 μm , while the inner diameter is found to be $\approx 30 \mu\text{m}$, on average. This unique structure is greatly beneficial, as it doubles the total surface area between Li and electrolyte by granting the diffusion of the electrolyte

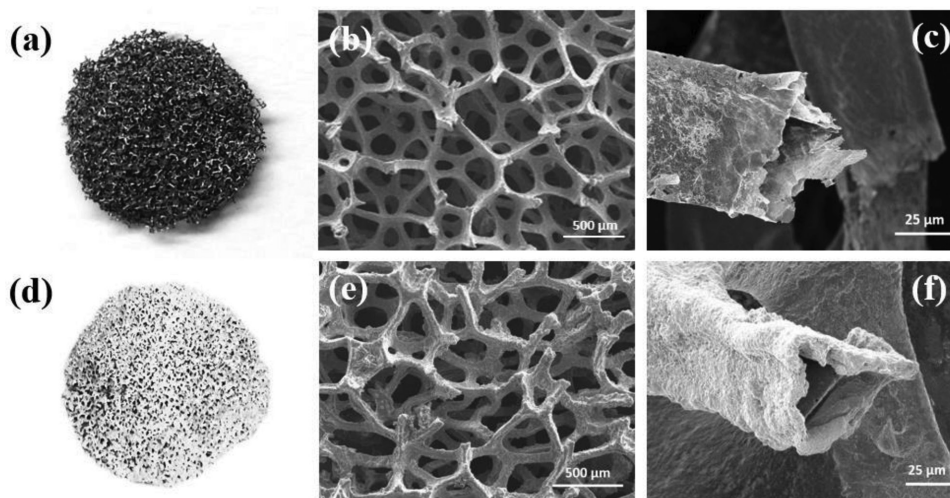


Figure 2. a) Snapshot for graphene foam before Li infusion. b) Graphene foam at low magnification after Ni etching. c) Hollow graphene foam at high magnification. d) Snapshot of for Li foam after infusion. e) Li foam at low magnification. f) Hollow Li foam under high magnification.

over both the inner and outer surfaces of the hollow foam. The structure allows optimum distribution of the electrolyte over the pores in between the foam, and through the inner surface as well. Also, the hollow and porous foam structure can accommodate the electrode volume change during charging/discharging.

To investigate the electrochemical performance of the Li foam, symmetric coin cells are used with two identical Li foam samples for both low and high coverages, as well as Li foil as a control cell. **Figure 3** shows the voltage hysteresis of the cells for 160 cycles at 1 and 4 mA cm⁻², both under 1 mAh cm⁻² charge. As obvious from Figure 3a, under 1 mA cm⁻², low- and high-coverage Li electrodes show higher electrochemical stability with low-voltage hysteresis compared with bare Li foil electrode. The inset figures reveal that the Li foil overpotential is widely varied during cycling, which is attributed to unstable electrochemical reactions over the surface during cycling. This is in agreement with previous reports, which show the preference of textured surfaces in improving the cell stability and reducing the dendrite formation.^[32]

On the other hand, under the high current density of 4 mA cm⁻², the difference in stability between the three structures became more distinct. The bare Li foil electrode starts to show a decrease in the overpotential at the beginning of cycling, which is related to the removal of the native oxide layer formed on the Li surface, which decreases the overall resistance and hence reduces the voltage overpotential. After 25 cycles, the bare Li foil shows an increase in the overpotential; then it

fluctuates before the voltage is completely dropped after 70 cycles as an indication of cell failure. These fluctuations are strongly attributed to unstable SEI on the Li surface during the stripping/plating cycles and are main reasons for dendrite formation and unstable performance for the electrode.^[30,36] Meanwhile, although the highly covered Li foam shows more stable performance than the bare Li, its overpotential is dropped after 110 cycles, which is attributed to gradual increase of dendrite formation on the surface, causing short circuit problems and cell failure. These findings support our claim and prove that highly Li covered structures still cannot suppress dendrite formation on the long term. This asserts that Li infusion with high rates and complete coverage need to be well controlled. Otherwise, it could produce nonuniform surface with random current density distribution, which enhances the dendrite formation and decreases the stability of the electrode. Figure 3b also reveals that low Li coverage electrode has promising performance, and the cell shows high stability under high current densities (4 mA cm⁻²), by which the cell retains cycling for more than 160 cycles without any fluctuation in the overpotential profile. Moreover, the low-covered samples have Li only infused over the graphene boundaries. This confines Li in a well-defined 3D structure that decreases the volume change during cycling. Also, it forms an optimum structure for uniform electrolyte coverage, with greatly enhanced surface area that decreases the local current density and limits the dendrite formation. These advantages give the superior electrode performance compared with its highly covered and bare Li foil electrode counterparts.

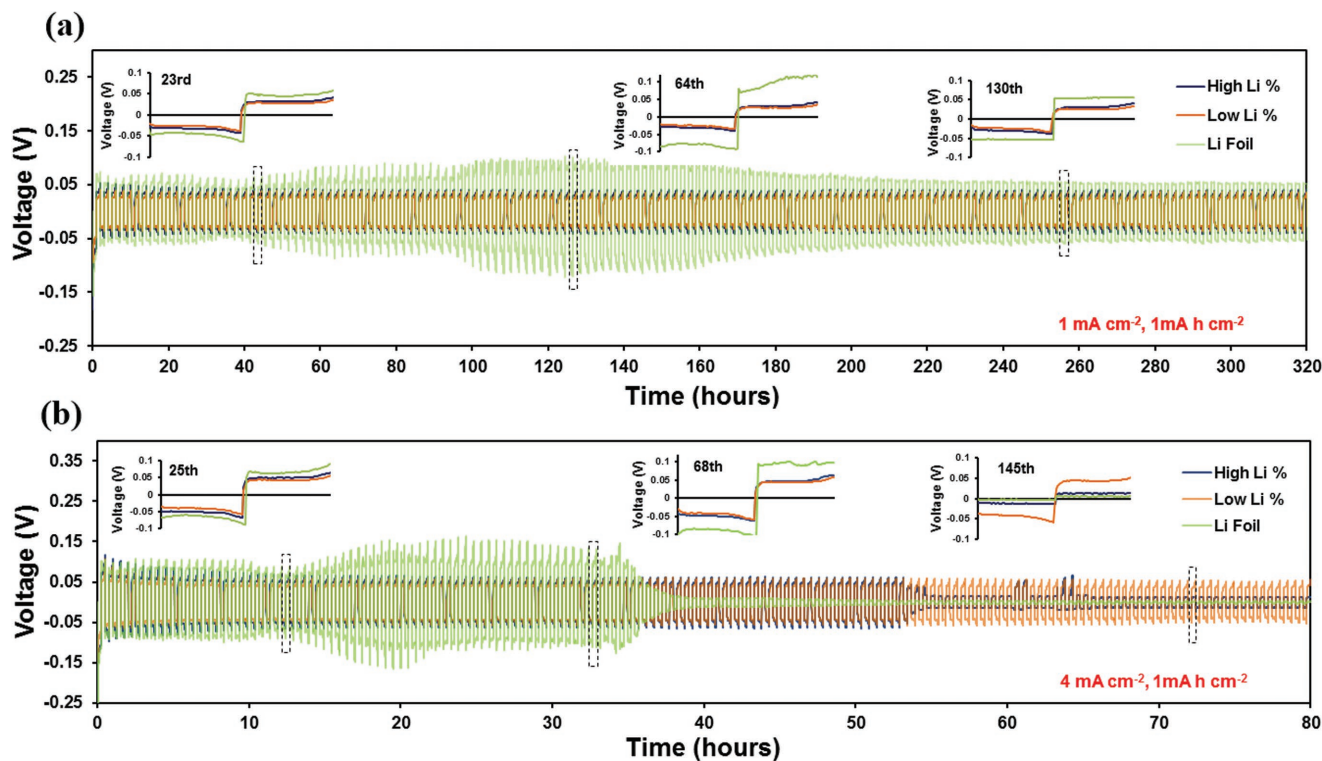


Figure 3. Cycling stability of identical symmetric cells for Li foil (green), high Li coverage (violet), and low Li coverage (orange). a) Cycling at low current density of 1 mA cm⁻² with 1 mAh cm⁻² cycling capacity; the inset shows the variation of the overpotential after 23, 64, and 130 cycles. b) Cycling at high current density of 4 mA cm⁻² with 1 mAh cm⁻² cycling capacity; the inset image shows the variation of the overpotential after 25, 68, and 145 cycles.

It should be noted that dendrite formation takes mainly two different shapes. In early stages of electrodeposition, mossy Li grows from its roots, which can be revealed by the movement of the dendrite tips.^[37] By the development of mossy Li, the salt concentration near the electrode surface starts to decrease.^[38] After a certain limit, dendritic Li starts to shoot out, which is the main type that causes short circuit and batteries failure problems. The time estimated for this process is determined by Sand's formula^[39]

$$t_{\text{Sand}} = \pi D_{\text{app}} \frac{(z_c c_0 F)^2}{4 (j t_a)^2} \quad (1)$$

where z_c is the cation charge number ($z_c = 1$ for Li^+), c_0 is the salt concentration at the electrolyte, F is Faraday's constant, J is the current density, $t_{\text{Li}} = 1 - t_a$ are the transference numbers of Li cations and associated anions, and D_{app} are the apparent diffusion coefficient for the electrolyte. It can be observed from Equation (1) that the time estimated for dendritic Li to shoot out can be increased by decreasing the current density distribution and/or increasing the cation mobility—or the transference number—for Li ions. The Li foam hollow structure introduced in this study can control two parameters: a) increasing the overall surface area for charging/discharging process which decreases the overall current density over the electrode surface, in contrast to Li foil and highly covered Li samples that have smaller surface area access to electrolyte^[39]; and b) increasing the mobility of Li cations in the electrolyte through the highly porous structure. This is beneficial for improving the cell stability and increasing the battery life cycle even under higher current density, which further reveals the preference of the hollow foam structure over bare Li foil electrode-based cells.

The high stability of the polarization curves for Li foam with low coverage compared to highly covered and bare Li foil counterparts can be further confirmed through electrochemical impedance spectroscopy (EIS) measurements for the three samples before and after cycling. **Figure 4a** shows the Nyquist plots for the samples before cycling. It should be noted that the high-frequency semicircle represents the charge interfacial resistance at the electrode/electrolyte interface, which also reflects the stability of the SEI layer, whereas the intersection

of the semicircle with the Re (z) axis represents the ohmic resistance of the cell. Li foil shows high interfacial resistance of 408 Ω , which is mainly attributed to the oxide layer formed on the Li foil electrodes. The highly Li covered electrode sample has interfacial resistance of 287 Ω . This high resistance is due to the high interfacial resistance at the interface as a result of nonuniform electrolyte distribution across the surface of the electrode. The Li foam under low coverage has the lowest resistance of 139 Ω compared with the other two structures, which is a clear evidence of more uniform SEI layer and better charge transport at the interface. **Figure 4b** shows the Nyquist plot of the three samples after 15 cycles, which is performed to produce more stable SEI layer and better charge transport after the first few cycles. It can be observed that the bare Li foil interfacial resistance is greatly reduced to 105 Ω , as a result of oxide layer removal after cycling. On the other hand, highly covered Li samples' resistance is further reduced to 35 Ω , while the interfacial resistance for Li foam under low coverage is reduced to only 13 Ω . The smaller charge transfer resistance further confirms that Li foam with low coverage has higher stability and better kinetics with favorable charge transport during stripping/plating.

To further understand the surface stability and morphology change during cycling, SEM images are taken after 100 cycles for each set of samples. **Figure 5a–c** show the surface morphology for bare Li under different magnifications. **Figure 5a** shows low-magnification image for Li foil electrode; the bare Li foil surface is found to have random peak and troughs across the surface, which distribute the current density in a random way. This leads to variation in the ionic flux density per unit area, by which dendrites show up with cycling. It is also more obvious from **Figure 5b** that dendrites exist with different densities across the surface. Under higher magnification (**Figure 5c**) severe dendrites can be observed. As expected, this is related to the nonuniform ionic flux during cycling, causing SEI instability and enhancing dendrite formation. **Figure 5d–f** reveal the high Li coverage foam under different magnifications. **Figure 5d** reveals that the foam pores are approximately blocked by high Li infusion with different thicknesses and random coverages. Moreover, dense dendrite formation over the foam surface can be detected at **Figure 5e**, which is also observed at **Figure 5f**,

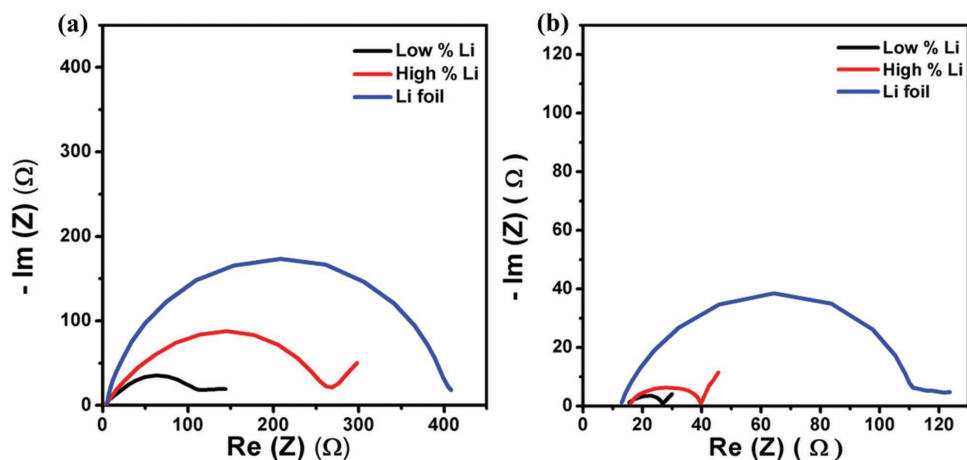


Figure 4. EIS for Li foil (blue), high Li coverage (red), and Li foam under low coverage (black). a) Before cycling and b) after 15 cycles.

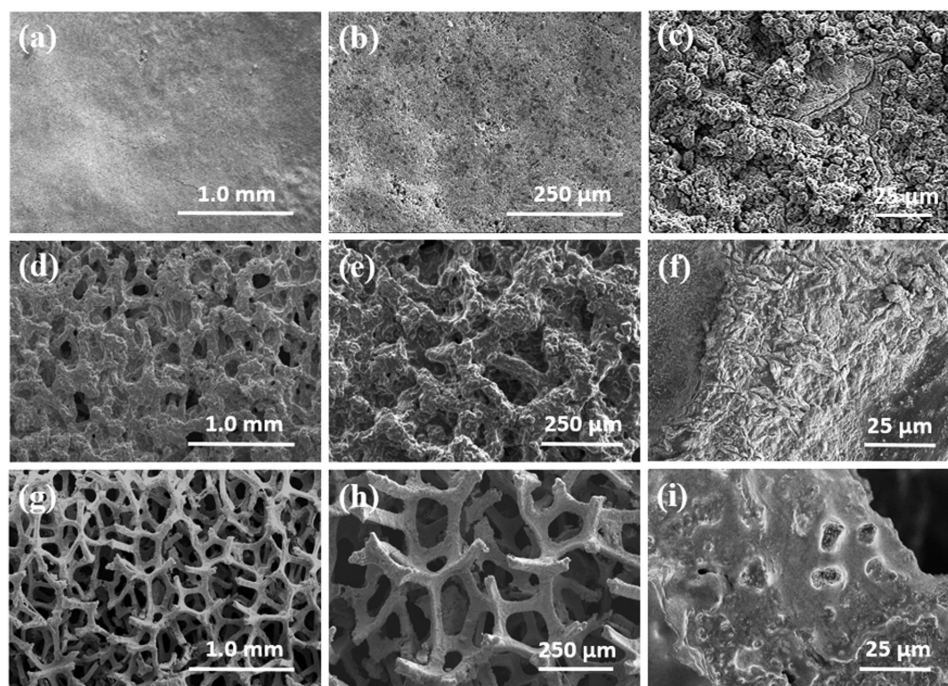


Figure 5. SEM images of the surface morphology of the three structures after 100 cycles under different magnifications. a–c) Li foil surface morphology, d–f) high-coverage Li structure, and g–i) Li foam under low coverage.

where dendrites are formed on the surface of the foam as well as the closed pore surface. This observation further asserts that highly and uncontrolled Li infusion inside the host still cannot suppress dendrites over long cycling, as it approximately fills all the pores with Li and prevents electrolyte from diffusing freely through the inner and outer surfaces of the foam. Figure 5g–i represent the morphology of Li foam structure under low coverage. Figure 5g shows exceptional morphological stability for Li foam after cycling, which is resulted from the controlled amount of Li infused inside the host that provides the minimum amount of Li needed for sufficient charging/discharging, with minimum possible volume change over long-term cycling. Also, from Figure 5h, large suppression of dendrite on the Li foam surface can also be detected, which is more clear under higher magnification (Figure 5i). This is related to the unique porous hollow structure and homogeneous Li coverage over the foam surface. Moreover, the highly porous morphology decreases the ionic resistance by providing high pathways for the ionic diffusion along the foam boundaries. These data further explain the difference in the stability between the three structures, where the rate of dendrite formation greatly varies for each morphology.

To measure the foam performance, full cell test is performed with LiFePO_4 as cathode, and either low-coverage Li foam or bulky Li foil as anodes. Cycling stability test is conducted under different current rates. As shown in Figure 6a, Li foam shows better rate capability with stable cycling and lower hysteresis compared with its Li foil counterpart. The foam exhibits larger capacity under high current rates ($\approx 30 \text{ mAh g}^{-1}$ at 10 C), whereas Li foil approximately exhibits only 3 mAh g^{-1} at 10 C. This is attributed to uniform Li stripping/plating on the foam structure, and even current density distribution over

the electrode surface compared with bare Li foil electrode, which becomes more clear under high charging/discharging rates.^[32,40] It should be mentioned that Li foil shows good stability at very low rates (0.2 C). According to Sand's model, this is attributed to the low chance of forming dendritic Li under low charging/discharging rates. However, the charging/discharging at such low rates is not suitable for most commercial applications, which limits the application of Li metal anode in secondary high-rate rechargeable batteries. The cycling stability is further confirmed by the coulombic efficiency for both Li foam and Li foil anode based cells. The efficiency was calculated as the ratio of the charge amount of complete Li dissolution to that of Li deposition for each anode. As shown in Figure 6b, Li foam shows large stability with high coulombic efficiency ($\approx 99.5\%$) over 200 cycles at 1 C charging/discharging rate. In contrast, Li foil shows instability and hysteresis in the coulombic efficiency with lower values. The higher coulombic efficiency for Li foam can also be related to the formation of stable SEI layer across the foam surface, which ensures long cycle life in such Li-metal-based batteries.^[41] Figure 6c,d reveal the voltage profiles for both anodes at 2 and 5 C charging/discharging rates. As shown in Figure 6c, Li foam acquires higher stability with flat voltage plateaux and lower overpotential at large specific capacity compared with Li foil electrode at 2 C. The difference becomes larger by increasing the charging/discharging rate to 5 C. This result is also consistent with the symmetric cell test discussed previously and confirms the improved stability and preference of the Li foam over other Li structures to be used under high charging/discharging rates.

In order to understand the effect of uniform electrolyte distribution on suppressing the formation of Li dendrites, density functional theory (DFT) calculations were performed for Li

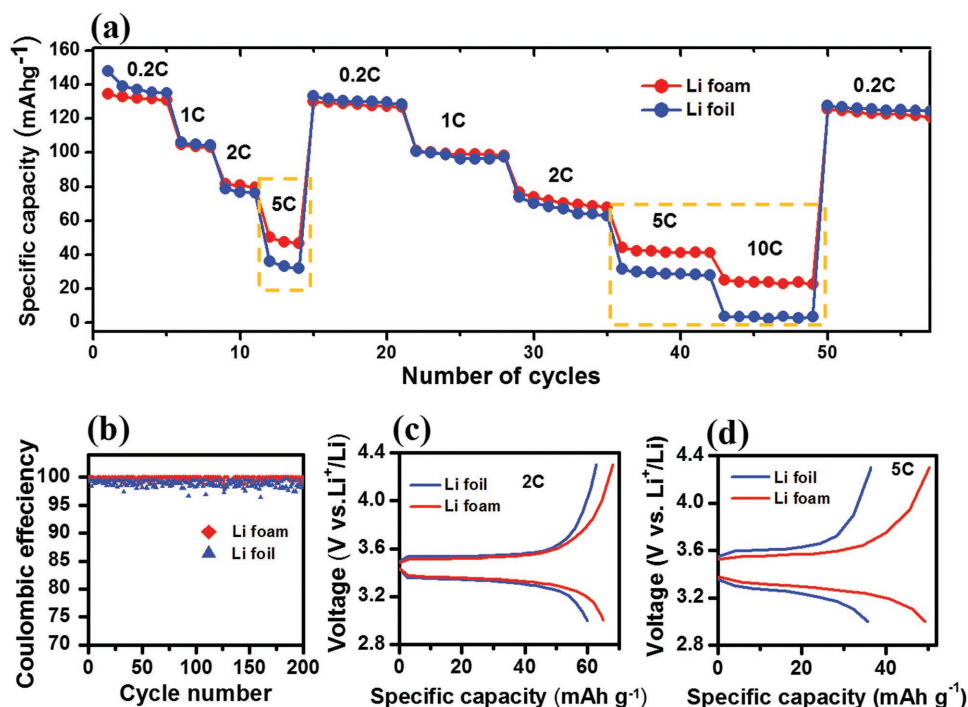


Figure 6. Electrochemical performance for LiFePO₄/Li foam (red) and LiFePO₄/Li foil (blue) full cell test. a) Rate capability under various rates from 0.2 to 10 C, b) coulombic efficiency calculated at 1 C, c,d) voltage profile comparison for each cell at 2 and 5 C, respectively.

atomic adsorption (adatom) on Li (100) surface in contact with electrolyte as shown in **Figure 7**. We chose the Li (100) surface as it has the lowest surface energy, which can accurately represent the Li metal surface.^[42] The formation energy of the Li adatom is calculated as

$$E_f = E(\text{Li}_{\text{atom}} + \text{surface}) - E(\text{surface}) - E(\text{Li}_{\text{atom}}) \quad (2)$$

where $E(\text{Li}_{\text{atom}} + \text{surface})$ and $E(\text{surface})$ are total energies of Li (100) surfaces with and without Li adatom, respectively. $E(\text{Li}_{\text{atom}})$ is the reference energy of Li atom, which can be chosen as the energy of bulk metal (this reference energy is canceled when comparing the formation energy). More detailed information can also be found in the Supporting Information. As can be observed from the calculations (Table S1, Supporting

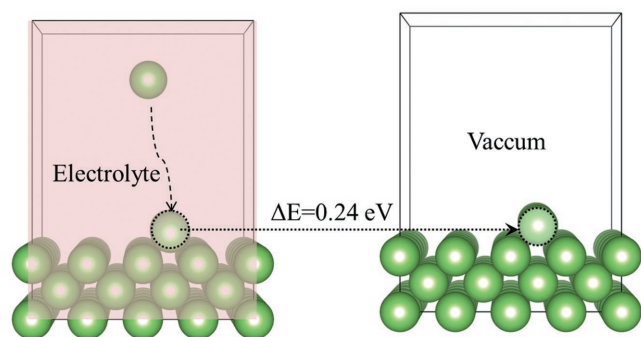


Figure 7. The schematics of Li adatom on Li (100) surface with and without electrolytes. The pink and white areas represent electrolyte and vacuum, respectively.

Information), the formation energy with Li ion adsorption is more stable by 0.24 eV at the presence of electrolyte in contact with Li metal surface. These results show that the variation in the Li contact will have a significant impact on the adsorption energy and thus the dendrite growth rate. In other words, when the electrolyte is uniformly distributed and has good accessibility over the electrode surface, such as in the hollow and porous Li foam, Li will grow uniformly and dendrite formation will be highly suppressed. This simulation result also further explains why the highly porous structure has better performance than its bulk and low porous Li structure counterparts.

In summary, we successfully demonstrated a novel structure design for Li metal electrodes in the form of hollow Li foam. The unique morphology of Li foam revealed high stability in symmetric cell test with low overpotential compared with bare Li foil electrode. The impedance measurements revealed that hollow Li foam has better charge transport and lower impedance compared with the highly covered Li and bare Li foil counterparts. Moreover, the morphology of the electrode after cycling confirmed the capability of hollow Li foam to suppress dendrite even under high current densities (4 mA cm⁻²), with large cycling stability over 160 cycles at the same current density. The full cell test is also performed using Li metal foam as anode and LiFePO₄ as cathode. Excellent rate capability of 138 mAh g⁻¹ at 0.2 C is achieved using Li foam, with high coulombic efficiency of ~99.5% for 200 cycles at 1 C. Finally, first principle calculations were performed on the hollow structure, which supported the experimental results by asserting uniform plating/during cycling on the hollow foam structure compared with its bare Li foil counterpart. We believe that the porous Li foam structure can provide

attractive alternative for Li metal foil electrodes. As it provides large stability and better electrochemical performance, which is critically demanded for energy storage devices in wide electrical applications nowadays.

Experimental Section

Preparation of Graphene Foam Framework (GF): The graphene foam was prepared by chemical vapor deposition method with 3D nickel (Ni) foam as template. First, Ni foam was annealed under argon and 5% hydrogen gas mixture flow. Second, CH₄ gas was introduced to the structure, then cooled down to room temperature under a continuous flow of argon and hydrogen gas. Third, the obtained graphene/Ni foam structure was immersed in a mixture of iron chloride (FeCl₃) (0.1 M) and hydrochloric acid (HCl) solution (1 M) for 30 min, in order to etch Ni and get the freestanding and hollow graphene foam. Finally, the structure was thoroughly cleaned by ethanol and left to dry in air.

Preparation of Li Foam Electrode (LF): The obtained graphene foam was first soaked in 1.0 M zinc nitrate (Zn(NO₃)₂) in ethanol for 5 min, then the structure annealed at 240 °C for 10 min. Afterward, the foam was transferred into an argon-filled glove box for Li melting. Li ribbons (99.9%, Sigma Aldrich) were scraped using blade in order to get rid of any surface oxide layer. After that, fresh Li metal was melted to 250 °C, at which graphene foam was put in contact with the molten surface. Li slowly starts to infuse through the structure, covering both the inner and outer surfaces of the graphene foam and forming a foam of Li 3D hollow structure. Finally, the structure was left to cool down before using it to assemble the battery cells.

Electrochemistry Characterization: For Li the stripping/plating cycling test, the electrodes were assembled with symmetric cell configuration into 2025-type coin cells (MTI). The electrodes used for this test were Li metal, Li foam, and fully covered graphene Li foam symmetric electrode pairs. For the full cell test, Li foam was used as anode electrode, while Li iron phosphate (LiFePO₄) was used as cathode, the active material was mixed with poly(vinylidene fluoride) and carbon black with a ratio of 8:1:1 in *N*-methyl-2-pyrrolidone solvent. The areal mass loading was (2.5 mg cm⁻²) for the cathode electrode. The electrolyte used in the test was (1 M) Li bis(trifluoromethanesulphonyl)imide in 1:1 v/v 1,3-dioxolane/1,2-dimethoxyethane with 2 wt% Li nitrate. The separator used in all cells was Celgard 2325 (25 μm). Galvanostatic cycling test was performed using LANDTH 8-channel tester. The EIS was conducted using Biologic VMP3 potentiostat.

Supporting Information

Supporting Information is available from the Wiley Online Library or from the author.

Acknowledgements

This research was financially supported by the start-up grant and Tier1 fund to H.Z. from Northeastern University. The authors also appreciate the use of the facilities at George J. Kostas Nanoscale Technology and Manufacturing Research Center at Northeastern. Y.L. thanks the start-up support from UT Austin. This work used computational resources sponsored by the DOE's Office of Energy Efficiency and Renewable Energy and located at the National Renewable Energy Laboratory, and the Texas Advanced Computing Center (TACC) at UT Austin.

Conflict of Interest

The authors declare no conflict of interest.

Keywords

charge distribution, dendrite suppression, density functional theory, ion diffusion, lithium metal anodes, porous lithium foams

Received: April 3, 2018

Revised: May 1, 2018

Published online:

- [1] H. Kim, G. Jeong, Y.-U. Kim, J.-H. Kim, C.-M. Park, H.-J. Sohn, *Chem. Soc. Rev.* **2013**, *42*, 9011.
- [2] W. Xu, J. Wang, F. Ding, X. Chen, E. Nasybulin, Y. Zhang, J.-G. Zhang, *Energy Environ. Sci.* **2014**, *7*, 513.
- [3] R. Cao, W. Xu, D. Lv, J. Xiao, J. G. Zhang, *Adv. Energy Mater.* **2015**, *5*, 1402273.
- [4] G. Zheng, S. W. Lee, Z. Liang, H.-W. Lee, K. Yan, H. Yao, H. Wang, W. Li, S. Chu, Y. Cui, *Nat. Nanotechnol.* **2014**, *9*, 618.
- [5] T. Ohzuku, Y. Iwakoshi, K. Sawai, *J. Electrochem. Soc.* **1993**, *140*, 2490.
- [6] C. K. Chan, H. Peng, G. Liu, K. McIlwrath, X. F. Zhang, R. A. Huggins, Y. Cui, *Nat. Nanotechnol.* **2008**, *3*, 31.
- [7] M. Armand, J.-M. Tarascon, *Nature* **2008**, *451*, 652.
- [8] J.-M. Tarascon, M. Armand, *Nature* **2001**, *414*, 359.
- [9] Y. Lu, Z. Tu, L. A. Archer, *Nat. Mater.* **2014**, *13*, 961.
- [10] S. Choudhury, R. Mangal, A. Agrawal, L. A. Archer, *Nat. Commun.* **2015**, *6*, 10101.
- [11] X. B. Cheng, T. Z. Hou, R. Zhang, H. J. Peng, C. Z. Zhao, J. Q. Huang, Q. Zhang, *Adv. Mater.* **2016**, *28*, 2888.
- [12] D. Zhou, R. Liu, Y. B. He, F. Li, M. Liu, B. Li, Q. H. Yang, Q. Cai, F. Kang, *Adv. Energy Mater.* **2016**, *6*, 1502214.
- [13] W. Luo, Y. Gong, Y. Zhu, K. K. Fu, J. Dai, S. D. Lacey, C. Wang, B. Liu, X. Han, Y. Mo, *J. Am. Chem. Soc.* **2016**, *138*, 12258.
- [14] W. Zhou, S. Wang, Y. Li, S. Xin, A. Manthiram, J. B. Goodenough, *J. Am. Chem. Soc.* **2016**, *138*, 9385.
- [15] X.-X. Zeng, Y.-X. Yin, N.-W. Li, W.-C. Du, Y.-G. Guo, L.-J. Wan, *J. Am. Chem. Soc.* **2016**, *138*, 15825.
- [16] J. Qian, W. A. Henderson, W. Xu, P. Bhattacharya, M. Engelhard, O. Borodin, J.-G. Zhang, *Nat. Commun.* **2015**, *6*, 6362.
- [17] X. Q. Zhang, X. B. Cheng, X. Chen, C. Yan, Q. Zhang, *Adv. Funct. Mater.* **2017**, *27*, 1605989.
- [18] Q. C. Liu, J. J. Xu, S. Yuan, Z. W. Chang, D. Xu, Y. B. Yin, L. Li, H. X. Zhong, Y. S. Jiang, J. M. Yan, *Adv. Mater.* **2015**, *27*, 5241.
- [19] J. Qian, W. A. Henderson, W. Xu, P. Bhattacharya, M. Engelhard, O. Borodin, J.-G. Zhang, *Nat. Commun.* **2015**, *6*, 6362.
- [20] L. Suo, Y.-S. Hu, H. Li, M. Armand, L. Chen, *Nat. Commun.* **2013**, *4*, 1481.
- [21] P. Bai, J. Li, F. R. Brushett, M. Z. Bazant, *Energy Environ. Sci.* **2016**, *9*, 3221.
- [22] Q. Yun, Y. B. He, W. Lv, Y. Zhao, B. Li, F. Kang, Q. H. Yang, *Adv. Mater.* **2016**, *28*, 6932.
- [23] L.-L. Lu, J. Ge, J.-N. Yang, S.-M. Chen, H.-B. Yao, F. Zhou, S.-H. Yu, *Nano Lett.* **2016**, *16*, 4431.
- [24] K. Xie, W. Wei, K. Yuan, W. Lu, M. Guo, Z. Li, Q. Song, X. Liu, J.-G. Wang, C. Shen, *ACS Appl. Mater. Interfaces* **2016**, *8*, 26091.
- [25] R. Mukherjee, A. V. Thomas, D. Datta, E. Singh, J. Li, O. Eksik, V. B. Shenoy, N. Koratkar, *Nat. Commun.* **2014**, *5*, 3710.
- [26] Y. Sun, G. Zheng, Z. W. Seh, N. Liu, S. Wang, J. Sun, H. R. Lee, Y. Cui, *Chem* **2016**, *1*, 287.
- [27] R. Zhang, X. B. Cheng, C. Z. Zhao, H. J. Peng, J. L. Shi, J. Q. Huang, J. Wang, F. Wei, Q. Zhang, *Adv. Mater.* **2016**, *28*, 2155.
- [28] J. R. Dahn, T. Zheng, Y. Liu, J. Xue, *Science* **1995**, *270*, 590.
- [29] S. S. Chi, Y. Liu, W. L. Song, L. Z. Fan, Q. Zhang, *Adv. Funct. Mater.* **2017**, *27*, 1700348.

- [30] Z. Liang, D. Lin, J. Zhao, Z. Lu, Y. Liu, C. Liu, Y. Lu, H. Wang, K. Yan, X. Tao, *Proc. Natl. Acad. Sci.* **2016**, *113*, 2862.
- [31] D. Lin, Y. Liu, Z. Liang, H.-W. Lee, J. Sun, H. Wang, K. Yan, J. Xie, Y. Cui, *Nat. Nanotechnol.* **2016**, *11*, 626.
- [32] S. S. Chi, Y. Liu, W. L. Song, L. Z. Fan, Q. Zhang, *Adv. Funct. Mater.* **2017**, *27*, 1700348.
- [33] L. Yu, N. L. Canfield, S. Chen, H. Lee, X. Ren, M. H. Engelhard, Q. Li, J. Liu, W. Xu, J. G. Zhang, *ChemElectroChem* **2018**, *5*, 761.
- [34] C.-P. Yang, Y.-X. Yin, S.-F. Zhang, N.-W. Li, Y.-G. Guo, *Nat. Commun.* **2015**, *6*, 8058.
- [35] Y. Liu, D. Lin, Z. Liang, J. Zhao, K. Yan, Y. Cui, *Nat. Commun.* **2016**, *7*, 10992.
- [36] G. Bieker, M. Winter, P. Bieker, *Phys. Chem. Chem. Phys.* **2015**, *17*, 8670.
- [37] J.-i. Yamaki, S.-i. Tobishima, K. Hayashi, K. Saito, Y. Nemoto, M. Arakawa, *J. Power Sources* **1998**, *74*, 219.
- [38] H. J. Chang, A. J. Illott, N. M. Trease, M. Mohammadi, A. Jerschow, C. P. Grey, *J. Am. Chem. Soc.* **2015**, *137*, 15209.
- [39] H. J. Sand, *London, Edinburgh, Dublin Philos. Mag. J. Sci.* **1901**, *1*, 45.
- [40] J. Heine, S. Krüger, C. Hartnig, U. Wietelmann, M. Winter, P. Bieker, *Adv. Energy Mater.* **2014**, *4*, 1300815.
- [41] W. Li, H. Yao, K. Yan, G. Zheng, Z. Liang, Y.-M. Chiang, Y. Cui, *Nat. Commun.* **2015**, *6*, 7436.
- [42] L. E. Camacho-Forero, T. W. Smith, S. Bertolini, P. B. Balbuena, *J. Phys. Chem. C* **2015**, *119*, 26828.